


RESEARCH ARTICLE OPEN ACCESS

Bistable Wetting States on a Smooth Surface

Mizuki Tenjimbayashi¹  | Shunto Arai²¹Research Center for Materials Nanoarchitectonics (MANA), National Institute for Materials Science, Tsukuba, Ibaraki, Japan | ²Research Center for Macromolecules and Biomaterials, National Institute for Materials Science, Tsukuba, Ibaraki, Japan**Correspondence:** Mizuki Tenjimbayashi (TENJIMBAYASHI.Mizuki@nims.go.jp)**Received:** 17 December 2025 | **Revised:** 16 March 2026 | **Accepted:** 25 March 2026**Keywords:** bistable wetting states | hydrophile–lipophile balance (HLB) | hydroxyl-terminated polydimethylsiloxane | non-textured surface | sticky/repellent states

ABSTRACT

Droplets on a non-textured surface typically exhibit a monostable wetting state, as represented by Young state. Here, we show that droplets can exhibit bistability without surface texture by tuning molecular interactions. We investigated the behavior of water droplets on a smooth substrate when immersed in oil. The oil contains hydrophilic interaction components, and their hydrophobic–hydrophilic balance was systematically varied. For oils with a specific hydrophobic–hydrophilic balance, droplet states bifurcate between repellent or sticky depending on the order of droplet casting and oil immersion. These states are neither transient nor one-off, indicating molecular interactions can create an energetic barrier separating the two states rather than surface textures. Under other oil conditions, the droplet remains monostable, either repellent or sticky, regardless of the order. This work advances the fundamental understanding of molecular effects on droplet behavior and expands surface design strategies in functional materials without compromising mechanical durability.

1 | Introduction

When a droplet is cast onto a solid surface, part of the droplet/solid surface is replaced by their interface, and a wide variety of shapes and adhesion modes, such as spreading [1], sticky [2], and super-repellent [3], can be obtained. In principle, droplets on smooth surfaces exhibit a single wetting state. According to Young's law [4], droplet shape, quantified with a static contact angle θ_s , depends on the balance of substance-specific interfacial energies between the three phases of the droplet, contacting solid surface, and surrounding media unless the balance changes due to an external field [5–7]. Contact angles fluctuate due to external disturbances and the mobility of the contact line. The maximum/minimum contact angle is observed when the contact line advances/recedes, yielding the advancing/receding contact angles $\theta_{a/r}$ [8]. The mobility of the contact line depends on the degree of surface heterogeneity. Most object surfaces are not perfectly homogeneous, at least on the

molecular scale [9]. However, a surface with a much smaller degree of heterogeneity than the droplet contact line length can be regarded as a non-patterned surface when we measure the contact angles at droplet scale magnification [10].

A droplet on a non-patterned surface exhibits a single inherent contact angle range, that is, a monostable state. When the surrounding media is air, the droplet shape follows Young's law [4], or completely spreads ($\theta_s \approx 0^\circ$) on the smooth substrate, depending on the signs of spreading coefficient S . When the surrounding media is a droplet-immiscible liquid, the three phases follow Young's law, or one of the liquids (droplet or surrounding liquid) completely spreads on the smooth substrate. When the surrounding liquid completely spreads (that is, droplet spreading coefficient under surrounding liquid $S_d < 0$), the droplet becomes completely spherical and exhibits $\theta_s \approx 180^\circ$ [11]. In these cases, these droplet states are monostable and can be observed separately.

This is an open access article under the terms of the [Creative Commons Attribution](https://creativecommons.org/licenses/by/4.0/) License, which permits use, distribution and reproduction in any medium, provided the original work is properly cited.

© 2026 The Author(s). *Advanced Materials Interfaces* published by Wiley-VCH GmbH

However, when the solid surface is nano- or microtextured, the droplet follows two branched states: (i) the droplet homogeneously infuses the texture (Wenzel state) [12] or (ii) the droplet makes limited contact with the outermost textured surface (Cassie state) [13]. While there have been suggestions to define Wenzel/Cassie intermediate states [14–16], the distinction between the Wenzel and Cassie states is basically whether the texture is infused by the droplet phase or the surrounding media. These states are observed not only in air but also in liquids [17, 18]. In the Wenzel state, the surface texture enhances the droplet–surface contact area, resulting in highly sticky droplets with $\theta_s \gg \theta_r$ [19]. In the Cassie state, the droplet–substrate contact area is smaller than the apparent contact area, and the adhesion force is smaller than that in Wenzel state, which results in $\theta_s \approx \theta_r$. The Wenzel and Cassie states coexisted on a textured surface, one of which is energetically favored. However, the energetic barrier for transitioning between two states exists owing to surface texture, which enables the observation of the other metastable state [20]. Thus, surface texture plays a significant role in the emergence of bistable states. Herein, we investigate whether molecular interactions at the interfaces can be substituted for surface texture in terms of the potential barrier of formation between the two states.

In this study, we show that two apparently different wetting states, which satisfy the contact angle feature of $\theta_s \approx \theta_r$ and $\theta_s \gg \theta_r$, can coexist on a smooth surface owing to molecular interactions. The observed states are neither transient, one-off, nor induced by external stimuli. We modulated the number of hydrogen bonds in three phases: a water droplet, a smooth silanized substrate, and oil with a hydrogen bonding moiety as the surrounding media. As a result of molecular-scale wettability modulation, quantified by the hydrophobic–hydrophilic balance (also known as the Hydrophile–Lipophile Balance, or HLB), we found that the bifurcation of the droplet states depends on the order of interface formation, that is, the order of droplet casting and oil immersion. The static and dynamic wettability features of these states were experimentally confirmed, and the underlying mechanism was studied on a molecular scale using interaction, thermodynamic, and force measurements. We also confirmed that bistable states can be extended to different substance combinations based on the proposed mechanism.

2 | Results and Discussion

2.1 | Bistable States on One Smooth Surface

A self-assembled silane monolayer regulates the surface chemistry of the substrate without texturing [21]. The probe surface was a glass substrate modified with a phenyl silane monolayer. The surface has no texture (Figure 1a), and atomic force microscopy (AFM) measurements quantified the surface root-mean-square roughness of $R_q = 0.41$ nm at the scan range of $20 \mu\text{m} \times 20 \mu\text{m}$ (Figure 1b). In addition to the hydrophobic phenyl group, the surface had hydrophilic silanol groups from glass and the hydrolysis of phenyl silane, as confirmed from the Fourier-transform infrared (FT-IR) spectrum (Figure S1). The water contact angle in air is $(\theta_s, \theta_r) = (80^\circ \pm 2^\circ, 61^\circ \pm 1^\circ)$. By changing the surrounding media from air to liquid state hydroxyl-terminated polydimethylsiloxane (PDMS–OH) with HLB = 0.12

[22], the water droplet behavior branched into sticky or repellent (Figure 1c,d). The applicable wetting states depend on the order of interface formation (Figure S2). On the one hand, the droplet cast on the probe surface after immersion in PDMS–OH within 30 s (denoted as the post-cast droplet) has a water contact angle of $(\theta_s, \theta_r) = (176^\circ \pm 1^\circ, 173^\circ \pm 1^\circ)$ (Figure 1c), exhibiting nearly perfect hydrophobicity but with observable “non-zero” water adhesion (Figure S3 and Movie S1). Here, a PDMS–OH layer was entrapped beneath the resting post-cast droplet, similar to a Cassie state. The layer was too thin to be observed because it was squeezed by the droplet. During motion, the layer becomes sufficiently thick to allow side-view observation at the droplet scale. This is because the layer thickness increases with the droplet sliding velocity, known as oleoplaning effect [11]. On the other hand, the droplet cast before the immersion (denoted as the precast droplet) exhibited a water contact angle of $(\theta_s, \theta_r) = (131^\circ \pm 4^\circ, 107^\circ \pm 2^\circ)$ (Figure 1d; Movie S2). In both cases, θ_a reaches nearly 180° , which means PDMS–OH spreads completely (that is, equivalent to the PDMS–OH receding angle being nearly 0°) to the probe surface as a liquid state and prevents contact line advance. Note that PDMS–OH is neither coated nor grafted to the substrate, which is confirmed by the constant water contact angle in air regardless of the repeated PDMS–OH immersion and rinsing (Figure S4). Moreover, the droplets were not in a transient state and maintained the observed wettability for a sufficiently long time (discussed in Section 2.3 Interfacial stability).

2.2 | Interfacial States

Branched wetting states are observed within a specific HLB range. Figure 2a shows photographs of water droplets cast onto the substrate before and after immersion in PDMS(OH) with different HLB values. PDMS (HLB = 0), PDMS–OH (HLB = 0.12), and PDMS–OH (HLB = 0.73) have similar surface tensions of $\gamma_0 \approx 19.8, 19.9$, and 21.4 mN/m, respectively, and viscosities of $\eta \approx 50, 40, 35$ mPa·s. Under PDMS, the post- and precast droplets exhibit similar contact angles of $(\theta_s, \theta_r) = (125^\circ \pm 4^\circ, 84^\circ \pm 4^\circ)$ and $(118^\circ \pm 4^\circ, 83^\circ \pm 5^\circ)$, respectively. Under PDMS–OH (HLB = 0.73), the post- and precast droplets exhibit contact angles of $(\theta_s, \theta_r) = (170^\circ \pm 1^\circ, 168^\circ \pm 4^\circ)$ and $(167^\circ \pm 2^\circ, 146^\circ \pm 4^\circ)$, respectively, with notably high θ_r values. In contrast, under PDMS–OH (HLB = 0.12), branched repellent/sticky droplet behavior was observed, as discussed above, with $(\theta_s, \theta_r) = (176^\circ \pm 1^\circ, 173^\circ \pm 1^\circ)$ and $(131^\circ \pm 4^\circ, 107^\circ \pm 2^\circ)$ for post- and precast droplets (Figure 1c,d).

The possible interfacial states of the PDMS-entrapped region and droplet–substrate contact region at the molecular scale are illustrated in Figure 2b,c, respectively. The former state is termed Configuration R (repellent) because the entrapped PDMS layer limits the droplet contact with the solid. The latter state is termed Configuration S (sticky) because the droplet forms direct contact with the substrate. We expected the composition of the two configurations under the droplet to differ depending on the surrounding media. In Configuration R, droplet–substrate contact is not formed, thereby increasing the droplet repellency. Under PDMS–OH (HLB = 0.73), most of the region beneath the droplet was in Configuration R, but not the entire region because droplet adhesion was observed (Figure S3 and Movie S1). Under PDMS, most of the region beneath the droplet was in Configuration S, and the droplet adhered to the substrate

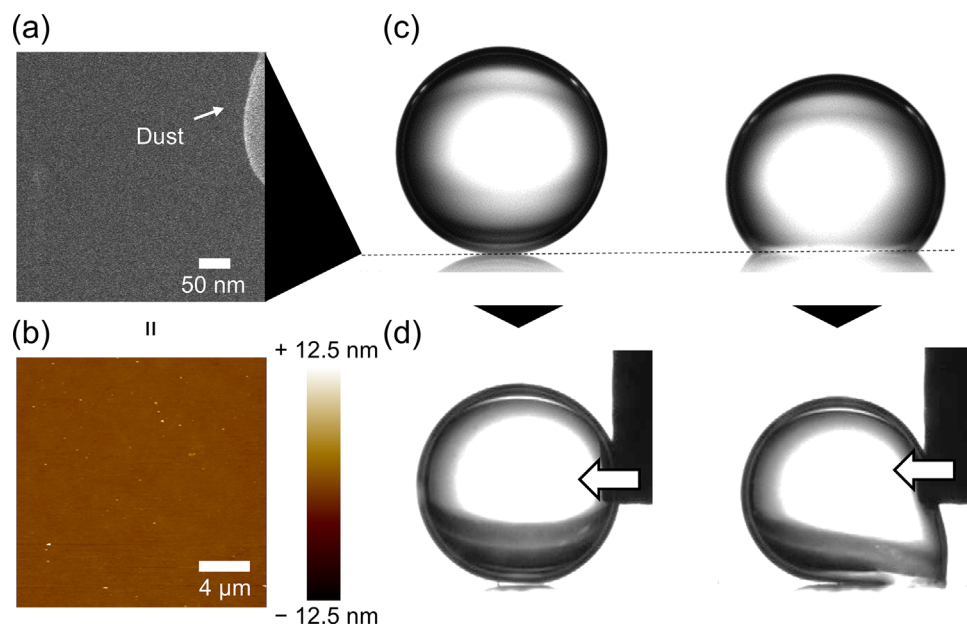


FIGURE 1 | Bifurcated wetting states on one smooth surface. (a, b) Field emission scanning electron microscopy (FE-SEM; top) and AFM (bottom) images of the phenyl silane-modified glass substrate surface. Dust was included in the FE-SEM image to confirm that the focus is correct. (c) Side-view photographs of two 5 μ L water droplets cast onto the one same substrate before (right) and after (left) immersing the substrate in PDMS-OH. (d) The adhesion behavior of the droplets in motion. Droplets were pushed with a Teflon needle parallel to the substrate.

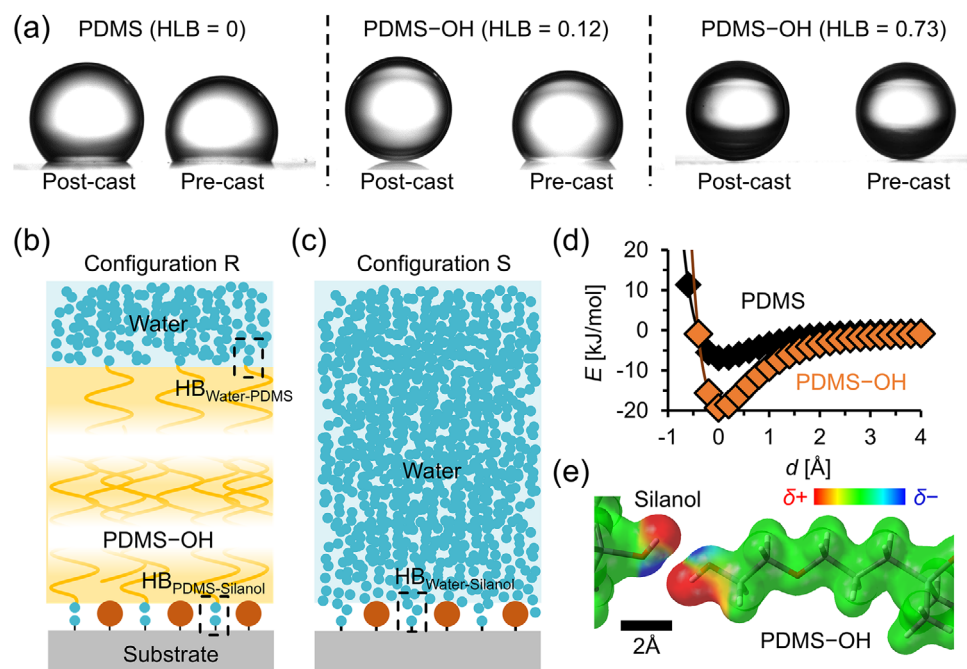


FIGURE 2 | Comparison of different interfacial states. (a) Photographs of pre-/post-cast water droplets under PDMS(-OH) with different HLBs. (b, c) Schematics of two interfacial states: (b) PDMS-OH is entrapped beneath the droplet and minimize the droplet substrate contact, denoted as Configuration R; (c) the droplet adheres to the substrate -OH area, denoted as Configuration S. Possible hydrogen bonding determines the preference between the two wetting states; hydrogen bonding between water and PDMS-OH ($\text{HB}_{\text{Water-PDMS}}$), PDMS-OH and silanol from the glass substrate and/or hydrolyzed silane ($\text{HB}_{\text{PDMS-Silanol}}$), or water and Silanol ($\text{HB}_{\text{Water-Silanol}}$). (d) Distance dependence of the intermolecular interaction energy between the -OH groups on the substrate surface silanol and the molecular end group of PDMS(-OH). (e) Electrostatic potential map of PDMS-OH in proximity to -OH groups on the substrate surface.

(Figure 2a, left), indicating that molecular interaction stabilized the PDMS–OH layer between the droplet and substrate. We consider this interaction to be hydrogen bonding between water and PDMS–OH ($HB_{\text{Water-PDMS}}$) and between PDMS–OH and the silanol interface ($HB_{\text{PDMS-Silanol}}$). Moreover, the oleophilic interactions between PDMS–OH and the substrate phenyl groups should also enhance the stability of the entrapped PDMS–OH. In Configuration S (Figure 2c), observed under PDMS and for the precast droplet under PDMS–OH (HLB = 0.12) (Figure 2a, left and center), the sticking property of the droplet is due to the direct contact between water and the substrate. Water molecules have a higher affinity for silanol groups than for phenyl groups because of possible hydrogen bonding with the substrate silanol groups ($HB_{\text{Water-Silanol}}$). See Note S1 [23, 24] for estimation of the $HB_{\text{Water-Silanol}}$ fraction in Configurations R and S.

As shown above, the specific configuration of the region beneath the droplet depends on the adhesion of PDMS(–OH) to the substrate beneath the water droplet through the possible formation of $HB_{\text{PDMS-Silanol}}$. To investigate this further, we calculated the intermolecular interaction energies at the PBE/6-311G** level of theory incorporating Grimme's dispersion correction [25] (see Methods section for details [26–29]). Figure 2d shows the interaction energy as a function of the distance between PDMS–OH and the silanol group. The potential well is shallow for PDMS but sufficiently large for PDMS–OH compared with the thermal fluctuation energy. The origin of this significant attractive interaction can be explained by electrostatic interactions. The electrostatic potential map between the end of PDMS–OH and the silanol group (Figure 2e) shows that the O (or H) of the silanol attracts the H (or O) of PDMS–OH, suggesting the formation of a hydrogen bond. Although the long-range interaction decays with distance from the substrate, it is still large compared to the thermal effect with a distance of 5–6 Å. This indicates that PDMS–OH can form sufficiently strong hydrogen bonds even with silanol groups covered by phenyl groups (approximately 4 Å in height), resulting in the formation of a stable PDMS–OH layer below the droplet, which is absent in the case of PDMS.

2.3 | Interfacial Stability

Figure 3a–c shows a comparison of the total energies of the two configurations under PDMS, PDMS–OH (HLB = 0.12), and PDMS–OH (HLB = 0.73), respectively. We calculated the difference in the unit area total interfacial energy γ_{total} of two configurations using $\Delta\gamma = \gamma_{\text{so}} + \gamma_{\text{ow}} - \gamma_{\text{sw}}$, where the subscripts s, o, and w denote substrate, PDMS(–OH), and water, respectively (see Methods section for details [30], Figure S5, and Table S1). Note that this value is intrinsically equivalent to the spreading coefficient S_d . We also confirmed that PDMS(–OH) does not dissolve in the water layer, and that the water–PDMS(–OH) interfacial energy is constant (Figure S6). Under PDMS, $\Delta\gamma = 28.2 \pm 2.8 \text{ mJ/m}^2$, indicating that Configuration S favored thermodynamically (Figure 3a). Thus, the water droplet contacts after immersion in PDMS transitioned from Configuration R to S, and the transition time was 13 s, which reflects the viscosity-dependent rupture of the PDMS layer below the droplet [31]. Under PDMS–OH (HLB = 0.12), Configuration S still is thermodynamically stable with $\Delta\gamma = 10.1 \pm 1.9 \text{ mJ/m}^2$ (Figure 3c). Because the viscosity of PDMS–OH (HLB = 0.12) is similar to that

of PDMS, the transition time is expected to be similar; however, the post-cast droplet maintained its shape for significantly longer. This implies that a considerable energetic barrier prevents the transition, which should mainly arise from the work required to detach PDMS–OH (HLB = 0.12) from the substrate underwater (that is, advance the contact line of water). Despite the difficulty in comparing the detachment force from the $\theta_a \approx 180^\circ$ (that is, PDMS receding contact angle $\approx 0^\circ$) for the precast droplets, we consider that the detachment work is higher for PDMS–OH (HLB = 0.12) than for PDMS owing to the $HB_{\text{PDMS-Silanol}}$. In contrast, under PDMS–OH (HLB = 0.73), Configuration R is thermodynamically stable, as indicated by $\Delta\gamma = -3.3 \pm 0.9 \text{ mJ/m}^2$ (Figure 3b). Despite the existence of an energetic barrier by $HB_{\text{Water-Silanol}}$, the precast droplet immediately switched from a sticky to a repellent state. This means the energetic barrier is too small to prevent the transition. In this case, the energetic barrier arises from the work required to detach (recede the contact line of) water from the substrate. Owing to the hydrophobicity (oleophilicity) of the substrate phenyl group, the water detachment is easier than the PDMS–OH detachment despite the existence of the $HB_{\text{Water-Silanol}}$. That is apparent from the $\theta_a \gg \theta_r$ for droplets in Configuration S. While this, the precast droplet under PDMS–OH (HLB = 0.12) did not switch because the droplet favors Configuration S (Figure 3c). The energy-level relationships of the configurations in Figure 3c were similar to those of the Cassie and Wenzel states observed in textured surfaces [32]. Notably, the energetic barriers to transitioning from configuration R to S should not differ significantly across these PDMS–OH systems, as HB sites in PDMS are sufficient to cover the silanol group on the substrate (see the discussion in the next section). Rather than that, the transition difficulty is dominated by the plus or minus sign of the $\Delta\gamma$. In the HLB = 0.12 case, to exhibit bistability, $HB_{\text{PDMS-Silanol}}$ should work to prevent transition from Configuration R to S. In this case, the $HB_{\text{PDMS-Silanol}}$ should be large enough to prevent the receding (advancing) of the PDMS (water). In the HLB = 0.73 case, to exhibit bistability, $HB_{\text{Water-Silanol}}$ should work to prevent transition from Configuration S to R. In this case, the $HB_{\text{Water-Silanol}}$ should be large enough to prevent the receding (advancing) of water (PDMS). This difference arises from the presence of a hydrophobic/oleophilic part.

2.4 | Droplet Adhesion Behavior

Although droplets in Configuration R (S) are repellent (sticky) under PDMS–OH (HLB = 0.12), the quantification of the adhesion force is challenging because the density of PDMS is comparable to that of the droplet. Thus, we estimated the droplet adhesion by measuring the critical sliding angle α of a PDMS-wrapped droplet (Figure S7) [33, 34], yielding $F \approx \rho V g \sin \alpha$, where $\rho \approx 0.997 \text{ g/mL}$ is the density of water, V is the droplet volume, and $g \approx 9.81 \text{ m/s}^2$ is the gravitational acceleration constant (Figure 4a). Figure 4b,c shows the sliding behavior of post- and precast droplets wrapped in PDMS–OH (HLB = 0.12) ($V = 5 \text{ }\mu\text{L}$). At a 1° tilt, the post-cast droplet in Configuration R slid off at a constant speed of $U = 36 \pm 11 \text{ }\mu\text{m/s}$, while the precast droplet in Configuration S did not slide off with the surface tilted at 90° . The apparent adhesion force difference depends on whether the droplet makes direct contact with the substrate. In Configuration R, the droplet–substrate contact is limited by PDMS(–OH); therefore, the contact line friction is negligible, and the adhesion

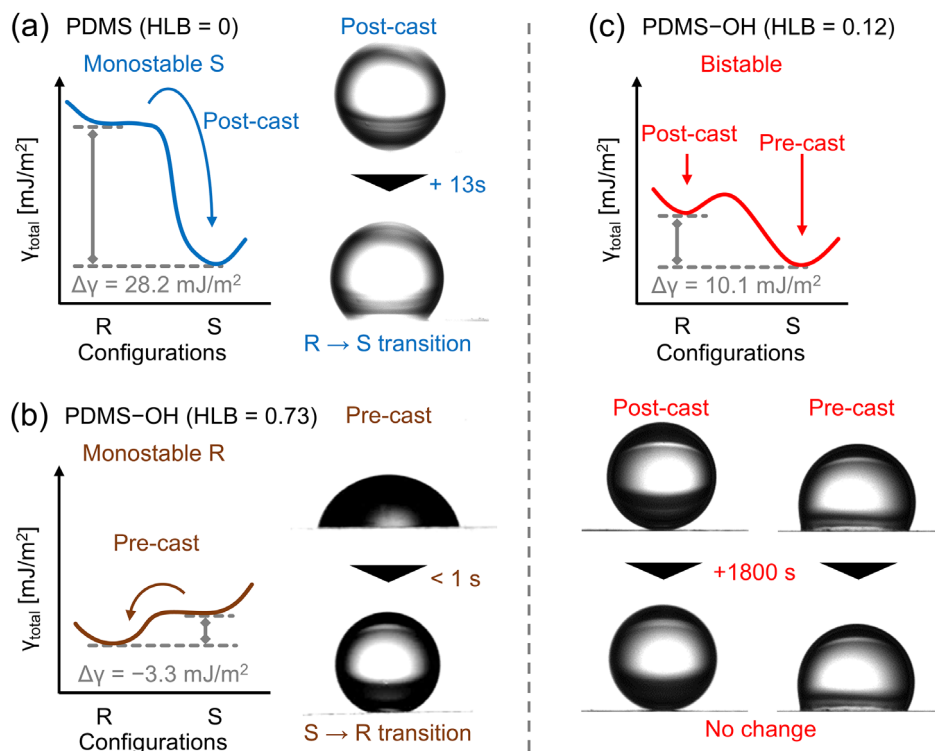


FIGURE 3 | Interfacial stability. Interfacial energy diagram and possible wetting transition of water droplet under (a) PDMS, (b) PDMS-OH (HLB = 0.73), and (c) PDMS-OH (HLB = 0.12). In (a)/(b), the post-/pre-cast droplet transitioned from repellent/sticky to sticky/repellent owing to their monostability. However, the pre-/post-cast droplet keeps sticky/repellent under PDMS-OH (HLB = 0.12) owing to the bistability.

force mainly originates from the viscous dissipation around the droplet [35]. In Configuration S, the droplet makes direct contact with the substrate, and the adhesion force corresponds to the contact line friction [36], especially on the rear side (note that $\theta_a \approx 180^\circ$).

Figure 4d shows the HLB effect on the droplet adhesion force. In this experiment, the droplet volume was $V = 20 \mu\text{L}$, which allowed us to measure the sliding angle values for all test droplets. Fine HLB adjustment was achieved by varying the mixing ratio of PDMS to PDMS-OH. In the PDMS (HLB = 0)-wrapped condition, with $\text{HB}_{\text{PDMS-Silanol}}$ absent, the adhesion force of the pre- and post-cast droplets was $F = 135.9 \pm 18.2$ and $110.2 \pm 9.0 \mu\text{N}$, respectively, not significantly different. However, the difference in the adhesion force between pre-/post-cast droplets increased with increasing HLB. Under the PDMS-OH (HLB = 0.02)-wrapped condition, obtained by diluting PDMS-OH (HLB = 0.12) with PDMS, the pre- and post-cast droplets exhibited $F = 27.2 \pm 15.4$ and $0.68 \pm 0.34 \mu\text{N}$, respectively. The droplet in Configuration R exhibited a mostly constant friction values of hundreds of nN. Furthermore, both the pre- and post-cast droplets transitioned from Configuration S to R, and the critical transition HLB differed for pre-/post-cast droplets. We defined the lower critical transition HLB observed for post-cast droplets as $\text{HLB}_{\text{LC}} = 0.01$ –0.02 and the upper critical transition HLB for precast droplets as $\text{HLB}_{\text{UC}} = 0.5$ –0.7. Branched wettability was observed between these critical HLBs, that is, $\text{HLB}_{\text{LC}} < \text{HLB} < \text{HLB}_{\text{UC}}$.

Next, we discuss the physical meaning of these transition points. The transition of precast droplets near HLB_{UC} is due to the change in the thermodynamically favored configuration, depending on

whether $\Delta\gamma$ is positive or negative. $\Delta\gamma$ decreases with increasing HLB (Figure S8) because γ_{ow} decreases with the increasing fraction of PDMS-OH by forming $\text{HB}_{\text{Water-PDMS}}$. The critical HLB for $\Delta\gamma = 0$ is estimated to be $\text{HLB} \approx 0.62$, which coincides with the experimentally obtained value of HLB_{UC} ($= 0.5$ –0.7). At $\text{HLB} < \text{HLB}_{\text{UC}}$ (that is, $\Delta\gamma > 0$), the interfacial state is in configuration S, and the contact line friction can be estimated using the Young–Dupré adhesion model $F_\gamma \sim \gamma_{\text{ow}}(1 + \cos\theta_r)$. This is reasonable because the adhesion force decreases with increasing HLB owing to the decrease in γ_{ow} . Here, slope fitting suggested $F \sim \text{HLB}^{-0.5}$, as shown by the black dashed line in Figure 4d. At $\text{HLB} > \text{HLB}_{\text{UC}}$ (that is, $\Delta\gamma < 0$), Configuration R is favored, and the adhesion force of the precast droplet drastically decreases.

The transition point of the post-cast droplets at HLB_{LC} depends on whether the OH groups in the PDMS can cap the substrate silanol groups, that is, to replace the $\text{HB}_{\text{Water-Silanol}}$ with $\text{HB}_{\text{Water-PDMS}}$. The number of hydrogen bonds available in PDMS(–OH) increases with increasing HLB. We considered HLB_{LC} to be the saturation point for $\text{HB}_{\text{PDMS-Silanol}}$. At $\text{HLB} < \text{HLB}_{\text{LC}}$, the amount of OH groups in the PDMS was insufficient to cover the substrate silanol groups; thus, the uncovered silanol groups result in the formation of $\text{HB}_{\text{Water-silanol}}$, and the droplets stick to the substrate. In this context, configurations R and S coexist beneath the post-cast droplets, akin to a “partial Wenzel state [37] or transitional state [16, 37],” and the total adhesion force is the sum of the $\text{HB}_{\text{Water-Silanol}}$ at the substrate–water contact region [38]. Under the assumption that (i) the water–silanol interface has negligible interfacial tension and (ii) that the Young–Dupré model is appropriate for molecular scale wetting, the unit adhesion force by $\text{HB}_{\text{Water-Silanol}}$ is $\sim F_\gamma [\theta_r \rightarrow 0]$. Moreover, the number density of

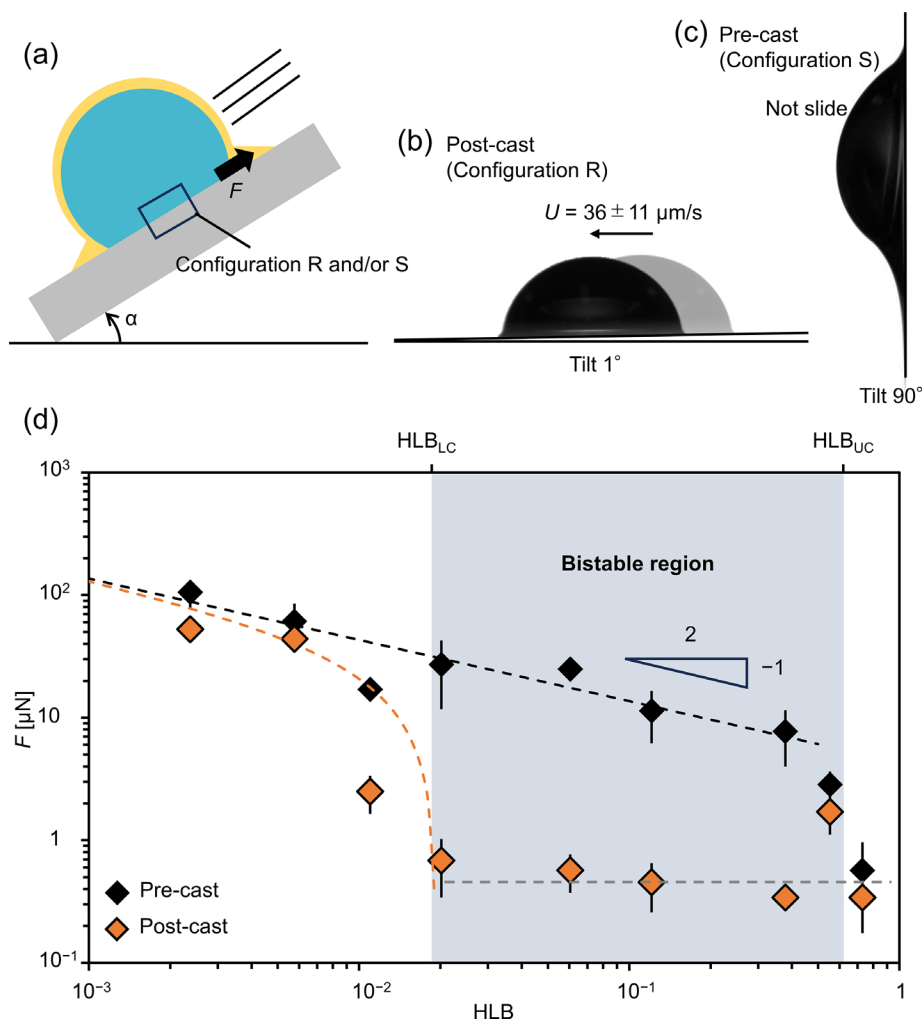


FIGURE 4 | Droplet adhesion behavior. (a) The experimental setup used to estimate the droplet adhesion force under PDMS(–OH). The water droplet was post-cast on the PDMS(–OH) lubricated substrate and tilted until the droplet started sliding. The adhesion force was quantified using the critical sliding angle α . A 5 μL water droplet wrapped with PDMS–OH ($\text{HLB} = 0.12$) in (b) Configuration R and (c) Configuration S. (d) Adhesion force evolution of wrapped 20 μL water droplets as a function of HLB. Dashed lines correspond to the fit of $F \sim \text{HLB}^{-0.5}$ (black), $F \sim \text{HLB}^{-0.5}(1 - \text{HLB}/\text{HLB}_{\text{LC}})$ (orange), and $F = \text{const.}$ (gray) to the experimental data.

$\text{HB}_{\text{Water-Silanol}}$ is proportional to the number of silanol groups that failed to be covered by OH groups in PDMS. Thus, we expect $F \sim F_{\gamma} [\theta_r \rightarrow 0] (1 - f_{\text{PDMS-OH}}/f_{\text{silanol}}) \sim \text{HLB}^{-0.5} (1 - \text{HLB}/\text{HLB}_{\text{LC}})$, where $f_{\text{PDMS-OH}}$ (f_{silanol}) is the number density of OH groups in PDMS (the substrate), which is approximately proportional to HLB (HLB_{LC}). Fitment of this model to the experimental data is shown by the orange dashed line in Figure 4d, affording $\text{HLB}_{\text{LC}} \approx 0.019$. At $\text{HLB} > \text{HLB}_{\text{LC}}$, the post-cast droplet favors Configuration R, and there is an excess of OH groups in PDMS that do not play a significant role in the droplet adhesion behavior. Thus, we obtain $F \approx \text{const}$ (gray dashed line).

2.5 | Extending Wettability Bifurcation to Different Material Combinations

Based on the proposed mechanism, we show that branched wettability can be extended to different material combinations (Figure 5). Branched wetting states were observed in various PDMS media containing different hydrogen-bonding terminating

groups. For example, molecular interactions between amino-terminated PDMS (PDMS-NH_2) and silanol are similar to those of PDMS–OH (Figure S9). Thus, we first studied the effect of HLB on the droplet adhesion force by substituting PDMS– NH_2 for PDMS–OH (Figure 5a). Branched wettability emerged at $\text{HLB} = 0.0008$ – 0.019 . Notably, bifurcation of the droplet shape was not observed when we used PDMS modified with non-hydrogen-bonding groups (Figure S10). The hydrophobic part of the surrounding medium is not limited to PDMS as long as the medium phase is water-immiscible and has a hydrogen-bonding group. We studied a fatty acid system using a mixture of 1-octadecene ($\text{C}_{18}\text{H}_{36}$) and oleic acid ($\text{C}_{17}\text{H}_{33}\text{COOH}$). Figure 5b shows the sliding angle of pre-/post-cast droplets ($V = 5 \mu\text{L}$) as a function of different HLB achieved by varying the mixing ratio of 1-octadecene to oleic acid. Branched wettability was observed in the region of $\text{HLB} = 0.3$ – 1.6 . Furthermore, hydrogen-bonding agents are not limited to liquids; a branched wettability system can be achieved by dissolving a solute in the liquid medium. We dissolved 1 wt.% octadecyl amine ($\text{C}_{18}\text{H}_{37}\text{NH}_2$) as a hydrogen bonding additive in 1-octadecene. After the dissolution, the HLB of the 1-octadecene

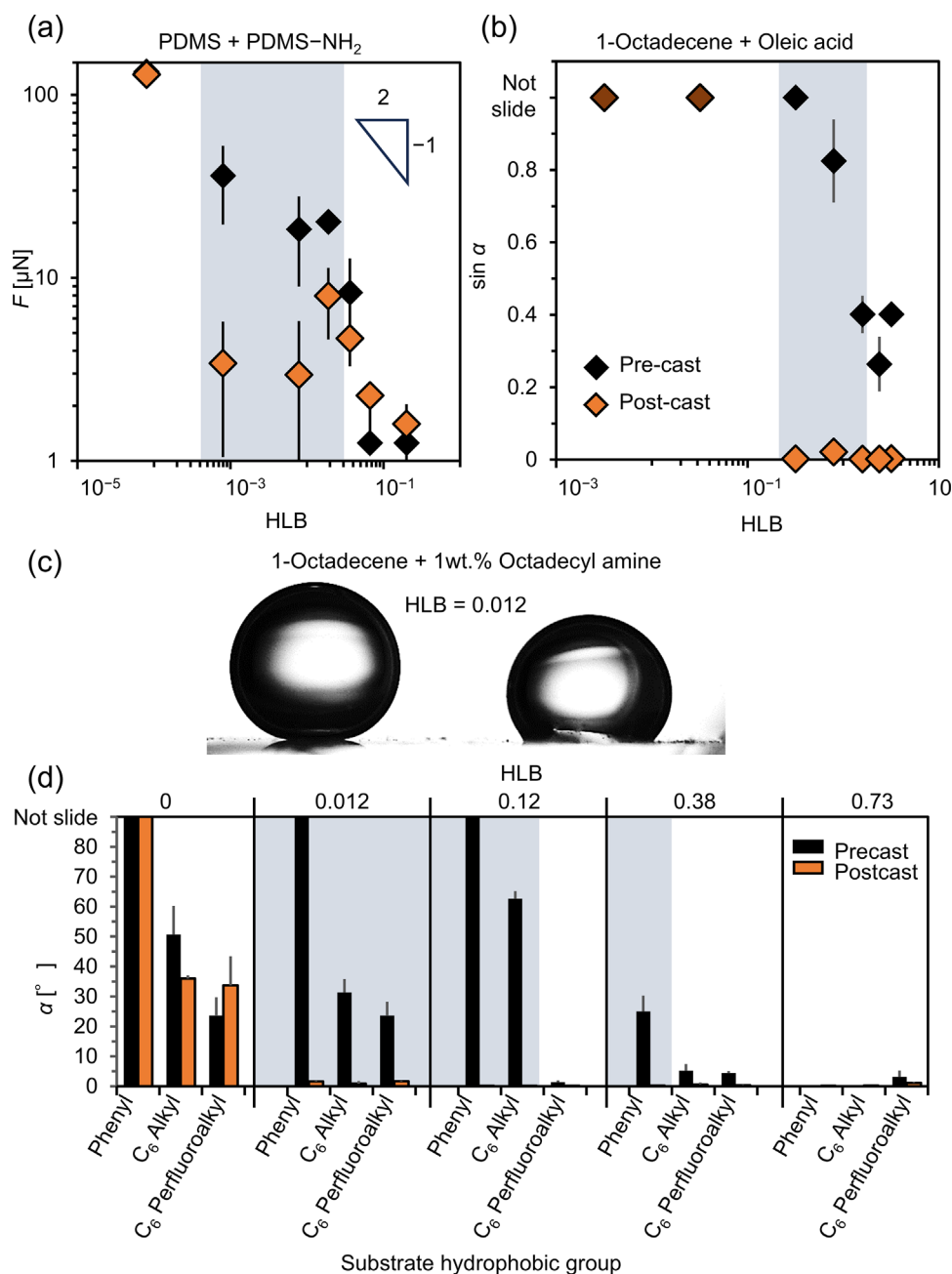


FIGURE 5 | Extending wettability bifurcation to different material combinations. (a) Adhesion force evolution of the wrapped 20-μL water droplets as a function of HLB for a mixture of PDMS and PDMS-NH₂. (b) Sliding angle of 5-μL water droplets under different mixtures of 1-octadecene and oleic acid. (c) Branched wettability of a water droplet under a mixture of 1 wt.% octadecyl amine and oleic acid. (d) Sliding angle of pre-/post-cast 5-μL water droplets on substrates with different hydrophobic moieties under a mixture of PDMS and PDMS-OH.

becomes 0.012. As shown in Figure 5c, branched wettability was observed. These results demonstrate the potential expansion of branched wettability to various surrounding media.

We also varied the hydrophobic part of the substrate from phenyl (C₆H₅-) to more hydrophobic alkyl (C₆H₁₃-, $R_q = 0.82$ nm) or perfluoroalkyl (C₄F₉C₂H₄-, $R_q = 1.14$ nm) groups while maintaining surface smoothness. With the increase of substrate hydrophobicity (that is, an increase in γ_{sw}), HLB_{UC} should decrease because of the decrease in $\Delta\gamma$. As expected, branched wettability was observed on all the probe surfaces. We found that HLB_{UC} decreased with increasing substrate hydrophobicity

in the order of perfluoroalkyl, alkyl, and phenyl modification (Figure 5d).

3 | Conclusion

The molecular-level tuning of the wettability balance enabled the observation of branched wetting states. Depending on the substrate and surrounding medium, a water droplet can be in a metastable state owing to the energetic barrier formed by molecular interactions, while another droplet is in a thermodynamically favored state. While this study mainly modulated the

hydrogen-bonding species in the surrounding medium, which determined the HLB, the insights gained can be expanded to the modulation of droplets, substrate surface chemistry, and molecular interactions other than hydrogen bonds. The observed droplet shape, adhesion behavior, and energy level of the configurations were analogous to those of Cassie and Wenzel droplets, regardless of the use of a smooth surface. In a Cassie-like state, a PDMS–OH (HLB = 0.12) layer too thin to be observed is entrapped beneath the resting droplet, whereas PDMS (HLB = 0) is squeezed out by a post-cast water droplet. In contrast to classical observations (that is, the case of $\Delta\gamma < 0$), it is energetically favored that PDMS–OH (HLB = 0.12) is squeezed out by the post-cast droplet. Therefore, $\text{HB}_{\text{Water-PDMS}}$ and/or $\text{HB}_{\text{PDMS-Silanol}}$ outcompete $\text{HB}_{\text{Water-Silanol}}$ to achieve surrounding media entrapment beneath the water droplet. In a Wenzel-like state, $\text{HB}_{\text{Water-Silanol}}$ form instead of $\text{HB}_{\text{PDMS-Silanol}}$. It is difficult to distinguish between a Wenzel-like state and a classical Young state in macroscopic wettability; however, the apparent difference is that the droplet in a Wenzel-like state exhibits $\theta_a \approx 180^\circ$, resulting in large contact angle hysteresis. Overall, this study found that a Cassie/Wenzel-like heterogeneous interfacial configuration appeared at the molecular scale, and the molecular effect resulted in macroscopic wettability features akin to those of Cassie/Wenzel droplets. We believe that a molecular-scale model interface analogous to the Cassie/Wenzel states is a powerful tool for understanding the molecular effects on droplet mobility [12, 39], adaptivity [40], micro-wetting [41], and nanofluidics [42]. These findings also provide guidance for the design of robust liquid repellents or capturing surfaces because surface nano/microscale textures typically suffer from low mechanical stability [43].

Acknowledgements

We acknowledge Dr. Gen Hayase for the FT-IR measurements, Ms. Makiko Yabune for the interfacial tension measurements, and general support from WPI-MANA.

Funding

Japan Society for the Promotion of Science (JSPS) KAKENHI (Grant No. 23K21042) (M.T.), 21H05234 (S.A.), 23K23201 (S.A.), LEADER (M.T.), Japan Science and Technology Agency (JST), FOREST grant JPMJFR223V (M.T.), PRESTO (Grant No. JPMJPR23N1) (S.A.).

Conflicts of Interest

None of the authors have a conflicts of interest to disclose.

Data Availability Statement

The data that supports the findings of this study are available in the supplementary material of this article.

References

1. S. Kalliadasis and H.-C. Chang, "Dynamics of Liquid Spreading on Solid Surfaces," *Industrial & Engineering Chemistry Research* 35 (1996): 2860–2874.
2. L. Feng, Y. Zhang, J. Xi, et al., "Petal Effect: A Superhydrophobic State With High Adhesive Force," *Langmuir* 24 (2008): 4114–4119.
3. T. Onda, S. Shibuichi, N. Satoh, and K. Tsujii, "Super-Water-Repellent Fractal Surfaces," *Langmuir* 12 (1996): 2125–2127.

4. T. Young, "An Essay on the Cohesion of Fluids," *Philosophical Transaction of the Royal Society London* 95 (1805): 65–87.
5. A. A. Papaderakis, M. Leketas, Z. Wei, et al., "Electrowetting of Carbon-Based Materials for Advanced Electrochemical Technologies," *Chem Electro Chem* 11 (2024): 202400143.
6. J. Li, N. S. Ha, T. L. Liu, R. M. Dam, and C. J. Kim, "Ionic-Surfactant-Mediated Electro-Dewetting for Digital Microfluidics," *Nature* 572 (2019): 507–510.
7. S. Kumar, P. Kumar, S. DasGupta, and S. Chakraborty, "Electrowetting of a Nano-Suspension on a Soft Solid," *Applied Physics Letters* 114 (2019): 073702.
8. H.-J. Butt, J. Liu, K. Koynov, et al., "Contact Angle Hysteresis," *Current Opinion in Colloid & Interface Science* 59 (2022): 101574.
9. S. Lepikko, Y. M. Jaques, M. Junaid, et al., "Droplet Slipperiness Despite Surface Heterogeneity at Molecular Scale," *Nature Chemistry* 16 (2024): 506–513.
10. J. Drelich, J. L. Wilbur, J. D. Miller, and G. M. Whitesides, "Contact Angles for Liquid Drops at a Model Heterogeneous Surface Consisting of Alternating and Parallel Hydrophobic/Hydrophilic Strips," *Langmuir* 12 (1996): 1913–1922.
11. D. Daniel, J. V. I. Timonen, R. Li, S. J. Velling, and J. Aizenberg, "Oleoplaning Droplets on Lubricated Surfaces," *Nature Physics* 13 (2017): 1020–1025.
12. R. N. Wenzel, "Resistance of Solid Surfaces to Wetting by Water," *Industrial & Engineering Chemistry* 28 (1936): 988–994.
13. A. B. D. Cassie and S. Baxter, "Wettability of Porous Surfaces," *Transactions of the Faraday Society* 40 (1944): 546.
14. S. Wang and L. Jiang, "Definition of Superhydrophobic States," *Advanced Materials* 19 (2007): 3423–3424.
15. K. Mądry and W. Nowicki, "Wetting Between Cassie–Baxter and Wenzel Regimes: A Cellular Model Approach," *The European Physical Journal E* 44 (2021): 138.
16. A. Giacomello, M. Chinappi, S. Meloni, and C. M. Casciola, "Metastable Wetting on Superhydrophobic Surfaces: Continuum and Atomistic Views of the Cassie–Baxter–Wenzel Transition," *Physical Review Letters* 109 (2012): 226102.
17. W. Ren, Z. Lian, J. Wang, J. Xu, and H. Yu, "Fabrication of Durable Underoil Superhydrophobic Surfaces With Self-Cleaning and Oil–Water Separation Properties," *RSC Advances* 12 (2022): 3838–3846.
18. X. Tian, V. Jokinen, J. Li, J. Sainio, and R. H. A. Ras, "Unusual Dual Superlyophobic Surfaces in Oil–Water Systems: The Design Principles," *Advanced Materials* 28 (2016): 10652–10658.
19. A. Lafuma and D. Quéré, "Superhydrophobic States," *Nature Materials* 2 (2003): 457–460.
20. G. Manukyan, J. M. Oh, D. van den Ende, R. G. H. Lammertink, and F. Mugele, "Electrical Switching of Wetting States on Superhydrophobic Surfaces: A Route Towards Reversible Cassie-to-Wenzel Transitions," *Physical Review Letters* 106 (2011): 014501.
21. M. Wang, K. M. Liechti, Q. Wang, and J. M. White, "Self-Assembled Silane Monolayers: Fabrication With Nanoscale Uniformity," *Langmuir* 21 (2005): 1848–1857.
22. W. C. Griffin, "Classification of Surface-Active Agents by 'HLB,'" *Journal of Cosmetic Science* 1 (1949): 311–325.
23. J. N. Israelachvili and M. L. Gee, "Contact Angles on Chemically Heterogeneous Surfaces," *Langmuir* 5 (1989): 288–289.
24. X. Zhao, B. Khatir, K. Mirshahidi, K. Yu, J. N. Kizhakkedathu, and K. Golovin, "Macroscopic Evidence of the Liquidlike Nature of Nanoscale Polydimethylsiloxane Brushes," *ACS Nano* 15 (2021): 13559–13567.
25. S. Grimme, S. Ehrlich, and L. Goerigk, "Effect of the Damping Function in Dispersion Corrected Density Functional Theory," *Journal of Computational Chemistry* 32 (2011): 1456–1465.

26. M. J. Frisch, G. W. Trucks, H. B. Schlegel, et al., Gaussian, Inc., Wallingford CT 16 (2016).
27. S. Tsuzuki and T. Uchimaru, "Accuracy of Intermolecular Interaction Energies, Particularly Those of Hetero-Atom Containing Molecules Obtained by DFT Calculations With Grimme's D2, D3 and D3BJ Dispersion Corrections," *Physical Chemistry Chemical Physics* 22 (2020): 22508–22519.
28. B. J. Ransil, "Studies in Molecular Structure. IV. Potential Curve for the Interaction of Two Helium Atoms in Single-Configuration LCAO MO SCF Approximation," *The Journal of Chemical Physics* 34 (1961): 2109–2118.
29. S. F. Boys and F. Bernardi, "The Calculation of Small Molecular Interactions by the Differences of Separate Total Energies. Some Procedures With Reduced Errors," *Molecular Physics* 19 (1970): 553–566.
30. A. Lafuma and D. Quéré, "Slippery Pre-Suffused Surfaces," *EPL (Europhysics Letters)* 96 (2011): 56001.
31. H. Xu, Y. Zhou, D. Daniel, et al., "Droplet Attraction and Coalescence Mechanism on Textured Oil-Impregnated Surfaces," *Nature Communications* 14 (2023): 4901.
32. D. Murakami, H. Jinnai, and A. Takahara, "Wetting Transition From the Cassie–Baxter State to the Wenzel State on Textured Polymer Surfaces," *Langmuir* 30 (2014): 2061–2067.
33. J. D. Smith, R. Dhiman, S. Anand, et al., "Droplet Mobility on Lubricant-Impregnated Surfaces," *Soft Matter* 9 (2013): 1772–1780.
34. T.-S. Wong, S. H. Kang, S. K. Y. Tang, et al., "Bioinspired Self-Repairing Slippery Surfaces With Pressure-Stable Omniphobicity," *Nature* 477 (2011): 443–447.
35. A. Keiser, P. Baumli, D. Vollmer, and D. Quéré, "Universality of Friction Laws on Liquid-Infused Materials," *Physical Review Fluids* 5 (2020): 014005.
36. G. H. McKinley, "Quantifying Contact Line Friction via Oscillating Droplet Dynamics," *Droplet* 1, (2022): 2–4.
37. K. A. Wier and T. J. McCarthy, "Condensation on Ultrahydrophobic Surfaces and Its Effect on Droplet Mobility: Ultrahydrophobic Surfaces Are Not Always Water Repellent," *Langmuir* 22 (2006): 2433–2436.
38. J. F. Joanny and P. G. de Gennes, "A Model for Contact Angle Hysteresis," *The Journal of Chemical Physics* 81 (1984): 552–562.
39. J. Zhang, K. Jia, Y. Huang, et al., "Intrinsic Wettability in Pristine Graphene," *Advanced Materials* 34 (2022): 2103620.
40. H.-J. Butt, R. Berger, W. Steffen, D. Vollmer, and S. A. L. Weber, "Adaptive Wetting—Adaptation in Wetting," *Langmuir* 34 (2018): 11292–11304.
41. D. Daniel, M. Vuckovac, M. Backholm, et al., "Probing Surface Wetting Across Multiple Force, Length and Time Scales," *Communications Physics* 6 (2023): 152.
42. L. Bocquet, "Nanofluidics Coming of Age," *Nature Materials* 19 (2020): 254–256.
43. X. Tian, T. Verho, and R. H. A. Ras, "Moving Superhydrophobic Surfaces Toward Real-World Applications," *Science* 352 (2016): 142–143.

Supporting Information

Additional supporting information can be found online in the Supporting Information section.

Supporting File: admi70495-sup-0001-SuppMat.docx.

Supporting Movie 1: admi70495-sup-0002-MovieS1.mp4.

Supporting Movie 2: admi70495-sup-0003-MovieS2.mp4.

Supporting Data: admi70495-sup-0004-DataFile.xlsx.